Mesoscopic simulations of the diffusivity of ethane in beds of NaX zeolite crystals: Comparison with pulsed field gradient NMR measurements

George K. Papadopoulos, Doros N. Theodorou, Sergey Vasenkov, and Jörg Kärger

Citation: J. Chem. Phys. **126**, 094702 (2007); doi: 10.1063/1.2567129
View online: http://dx.doi.org/10.1063/1.2567129
View Table of Contents: http://jcp.aip.org/resource/1/JCPSA6/v126/i9
Published by the American Institute of Physics.

Mesoscopic simulations of the diffusivity of ethane in beds of NaX zeolite crystals: Comparison with pulsed field gradient NMR measurements

George K. Papadopoulos[a),b)] and Doros N. Theodorou[a),c)]
School of Chemical Engineering, National Technical University of Athens, GR 15780 Zografou Campus, Athens, Greece

Sergey Vasenkov
Department of Chemical Engineering, University of Florida, Gainesville, Florida 32611

Jörg Kärger
Universität Leipzig, Abteilung Grenzflächenphysik, Linnéstrasse 5, D-04103 Leipzig, Germany

(Received 4 December 2006; accepted 18 January 2007; published online 2 March 2007)

Mesoscopic kinetic Monte Carlo simulations and pulsed field gradient nuclear magnetic resonance (PFG NMR) measurements are compared in order to investigate the transport of ethane in a bed of NaX crystals. A novel molecular mechanics particle-based reconstruction method is employed for the digital representation of the bed, enabling for the first time a parallel study of the real system and of a computer model tailored to reproduce the void fraction, particle shape and average size of the real system. Simulation of the long-range diffusion of ethane in the bed over the Knudsen, transient, and molecular diffusion regimes is consistent with the PFG NMR measurements in yielding tortuosity factors which depend upon the regime of diffusion; more specifically, tortuosity factors defined in the conventional way are higher in the Knudsen than in the molecular diffusion regime. Detailed statistical analysis of the computed molecular trajectories reveals that this difference arises in a nonexponential distribution of the lengths and in a correlation between the directions of path segments traversed between collisions with the solid in the Knudsen regime. When the Knudsen tortuosity is corrected to account for these features, a single, regime-independent value is obtained within the error of the calculations. © *2007 American Institute of Physics*.
[DOI: 10.1063/1.2567129]

I. INTRODUCTION

The study of transport phenomena in porous materials via both experiment and theory has a rich past due to its immense importance in processes such as the movements of petroleum and natural gas in porous strata, diffusion of water in plants or soil, and applications such as chromatography, catalysis, filtration, and sorption separations. Fick's first establishment of a phenomenological description for the diffusion of matter has been developed to a high degree of sophistication in the treatment of a wide range of problems, involving both transient and steady states of transport and diverse boundary and initial conditions.[1] A collection of topics from classical studies of diffusion and flow of fluids through porous media can be found in Refs. 2–6.

The coexistence of different length scales and complex connectivities in the space available for molecular motion inside real porous media introduces a significant structural dependence in the diffusion mechanism; as a consequence, theoretical equations derived to describe diffusion in simple idealized model systems (e.g., parallel pore models) are often inadequate for describing experimental measurements. Theory must be elaborated, or even totally revised, in order to capture the effects of the geometric complexity of real pore structures on the transport mechanism. A first study of this kind is the calculation of the effective conductivity of a suspension of randomly distributed spheres due to Maxwell.[4]

Computer-aided research on transport in pores has made an enormous progress over the last years based on geometric representations of the real medium with models such as bundles of capillaries, slits, or networks thereof with prescribed size distributions and connectivity, suspensions of spheres, fibers, or combinations thereof,[2,4,7–9] up to more abstract representations such as the dusty-gas model.[6] In early work, diffusion was typically analyzed theoretically in a model system of simple geometry and then the effective diffusivity in the real medium was expressed in terms of the theoretical value by means of suitable structure factors.[2,10] More recent computational studies have involved direct calculation of the trajectories of diffusers from the Knudsen up to the molecular diffusion regime by means of kinetic Monte Carlo simulation, in model pore structures comprising random assemblages of spheres, capillaries, or both of them in coexistence.[8,9,11–14]

Though easy to apply, the aforementioned approaches to the porous structure suffer from lack of precise knowledge of the spatial distribution and connectivity of solid and void spaces with respect to a particular microporous material; this knowledge is of crucial importance for studies aiming at the modeling of diffusion under confinement. Moreover, the

[a)]Authors to whom correspondence should be addressed.
[b)]Electronic mail: gkpap@chemeng.ntua.gr
[c)]Electronic mail: doros@central.ntua.gr

structural oversimplifications hinder the prospect of a rational coupling between simulation results and experimental measurements for a given system.

More sophisticated representations which do not invoke idealized model assumptions have appeared in the literature, which involve three-dimensional stochastic reconstruction of the pore matrix, based on digitized experimental micrographs constructed from image analysis of scanning, transmission or high-resolution electron microscopy, atomic force or fluorescence confocal optical microscopy, or x-ray tomography outputs.[15,16]

The objective of the present work is the investigation, at both a theoretical and an experimental level, of the "long-range" macropore diffusion of gases through zeolite beds. In particular, the transport of ethane in a bed of faujasite zeolite crystals (NaX) is studied by means of pulsed field gradient nuclear magnetic resonance (PFG NMR) and kinetic Monte Carlo (KMC) simulation. The digitally reconstructed bed of NaX employed in the simulation is tailored in order to reproduce the porosity, shape, and size of the zeolite crystallites in the real medium using a novel molecular mechanics simulation method. To our knowledge, this is the first time that the effect of the detailed morphology of the porous medium is examined via simulation, allowing a direct comparison with the PFG NMR measurements. Of particular interest is the question whether macropore diffusion in the Knudsen and molecular regimes can be described through the same tortuosity factor.

II. DIFFUSIVITY AND MOLECULAR TRAJECTORIES

In a three-dimensional isotropic molecular system the diffusion arising from the random thermal motion of molecules can be quantitatively expressed via Fick's second law in terms of a time dependent density field, $c(\mathbf{r},t)$, as follows:

$$\frac{\partial c(\mathbf{r},t)}{\partial t} = \nabla \cdot D(c)\, \nabla\, c(\mathbf{r},t), \tag{1}$$

where $\mathbf{r}$ denotes position vector, and $D(c)$ is in general a density-dependent transport diffusivity.

In cases where the concentration dependence of the diffusivity can be neglected, the solution of Eq. (1) with initial condition a delta function, at the origin takes the form of a Gaussian function,

$$P(\mathbf{r},t) = \frac{1}{(4\pi Dt)^{3/2}} \exp(-\mathbf{r}^2/4Dt). \tag{2}$$

The same form was obtained by Einstein in his seminal analysis of self-diffusion.[17] The distribution of Eq. (2) expresses the probability that, after a certain time t, a random walker starting at the origin and executing a succession of uncorrelated jumps in three-dimensional space will have attained a displacement $\mathbf{r}$. If the distribution of jump lengths has a finite second moment, for a time t that is long in comparison to the mean time between jumps the Gaussian form, Eq. (2), applies. Direct integration of Eq. (2) gives Einstein's equation, which relates the mean square molecular displacement (MSD, the second moment $\langle \mathbf{r}^2(t) \rangle$ of the Gaussian distribution of position vectors over time t), with the diffusivity in a three-dimensional (3D) system, i.e.,

$$\langle \mathbf{r}^2(t) \rangle = 6Dt. \tag{3}$$

Thus, the validity of relation (2) and hence of Eq. (3) only requires a random uncorrelated sequence of rectilinear steps, namely, a topologically homogeneous medium. However, in studies of diffusion in porous solids or beds of particles, the spatial distribution of molecules deviates from the Gaussian form of Eq. (2); Eq. (3) can apply only when the mean square displacement of sorbate molecules during the observation time is large enough for motion to be diffusive, and at the same time small in relation to the length scale of the particular homogeneous region inside the porous medium where transport is described by the diffusion coefficient D. In catalytic beds of zeolite crystals, this situation is met by microscopic methods for the evaluation of intracrystalline diffusion, such as quasielastic neutron scattering measurements and atomistic molecular dynamics simulations;[18] these methods operate on time scales of less than 1 μs and time scales of less than 10 nm, which are smaller than typical crystal sizes (1–100 μm) and even than typical distances between defects in zeolite crystals. Thus, the microscopic methods yield self—or transport diffusivities which are representative of motion in an essentially perfect crystalline structure. On the other hand, in the long-range diffusion regime,[17] which constitutes the focus of the present study, molecular displacements well exceed the crystal dimensions. Therefore, the system cannot be further treated as homogeneous over the length and time scales probed and Eqs. (2) and (3) can only be thought of in connection with an *effective* diffusivity for the porous medium.[19]

To overcome the problem of heterogeneity in pore systems, the distribution of molecular displacements may still be considered Gaussian with the MSD in Eq. (3) being related to the effective diffusivity, D_{eff}. If the sorbed molecules are envisioned as spending some of their time inside the zeolite crystals and the rest in the intercrystalline space, the displacement vectors in the two environments being completely uncorrelated to each other, then we can write[17]

$$D_{\text{eff}} = \frac{\langle \mathbf{r}^2(t) \rangle_{\text{intra}}}{6t} + \frac{\langle \mathbf{r}^2(t) \rangle_{\text{inter}}}{6t}. \tag{4}$$

With p_{intra} and p_{inter} being the number fractions of molecules present in the crystals and in the intercrystalline pore phase, respectively, it follows[17]

$$D_{\text{eff}} = p_{\text{intra}} D_{\text{intra}} + p_{\text{inter}} D_{\text{inter}}. \tag{5}$$

The quantities p_{intra} and p_{inter} are related to the concentrations c_{intra} and c_{inter} through

$$p_{\text{intra}} = (1-\phi)c_{\text{intra}}/c, \quad p_{\text{inter}} = \phi c_{\text{inter}}/c,$$

where ϕ is the porosity (void space fraction) of the bed and c is the total concentration in the bed,

$$c = \phi c_{\text{inter}} + (1-\phi)c_{\text{intra}}.$$

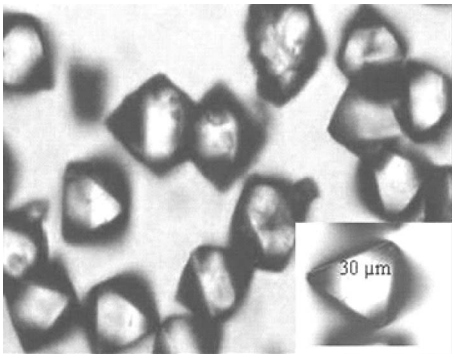

FIG. 1. Optical microscopy picture of octahedral NaX crystals; the inset depicts the mean edge size used in the simulation.

In the present work, the experimentally found conditions are such that $p_{\text{intra}} \gg p_{\text{inter}}$ and $D_{\text{intra}} \ll D_{\text{inter}}$ (negligible intracrystalline mobility). In addition, $D_{\text{intra}} \ll p_{\text{inter}} D_{\text{inter}}$, and Eq. (5) reads

$$D_{\text{eff}} = p_{\text{inter}} D_{\text{inter}} \tag{6}$$

It is instructive to note at this point that the unlikely case for zeolites of $D_{\text{intra}} \gg p_{\text{inter}} D_{\text{inter}}$ (high intracrystalline mobility) also leads to the approximation of Eq. (6).[17] This is explainable on the basis of the negligible contribution of intracrystalline diffusion to the overall resistance to mass transfer; once in the solid phase, a molecule quickly explores the entire crystal in which it is confined and transport through the bed is rate determined by the diffusivity in the interparticle (gas phase) region.

PFG NMR in the long-range diffusivity regime measures an effective diffusion coefficient $D_{\text{eff}} \equiv D_{\text{LR}}$, whereas kinetic Monte Carlo simulation in this work computes directly the interparticle diffusivity D_{inter}, assuming no entry into the zeolite crystals.

III. METHODOLOGY

A. Digital reconstruction of the NaX bed

A new reconstruction method is presented in this section, designed for cases where the porous medium under investigation consists of particles of known shape and size distribution. On the computer, such a medium is represented as a collection of particles obeying these distributions, with prescribed porosity, in detailed mechanical equilibrium. In the new algorithm, the particles are represented as collections of soft repulsive spheres with progressively increasing resolution. The material configuration is arrived at through a series of energy minimizations (molecular mechanics) at constant particle number density. In our case, the beds consist of octahedral crystals (see Fig. 1). Based on the measured bed density of 590 kg m^{-3} and the crystal density of 1530 kg m^{-3}, the bed porosity is $\phi = 0.6$. Furthermore, the mean crystal size (edge length of the octahedra) is 30 μm.

In the computer reconstruction, each octahedron is represented as a rigid collection of soft repulsive spheres. The purely repulsive potential active between all pairs of spheres belonging to different octahedra is described by the Lennard-Jones 6-12 expression up to a distance of 0.94σ, by a quintic spline[20,21] for distances between 0.94σ and 1.04σ, and is identically equal to zero for distances beyond 1.04σ. The first and second derivatives of the potential are continuous, ensuring good behavior during the minimizations.[20,21]

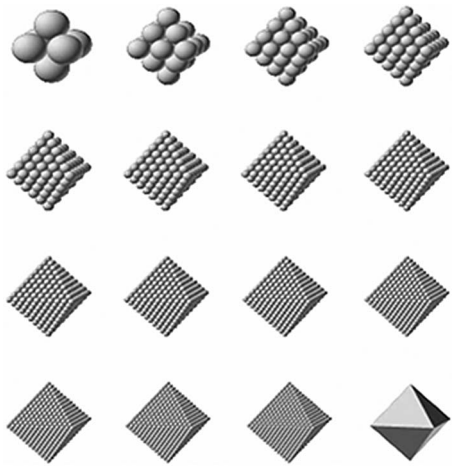

FIG. 2. Stages of successive representations of the octahedral object starting from $G=1$ (top left) and ending at $G=15$ (penultimate structure at the bottom).

Initially, only a single soft sphere is used to represent each crystal (generation 0). The volume of the sphere, calculated on the basis of the collision diameter σ, is taken equal to that of the entire octahedral crystal. N spheres are placed in a cubic domain of volume V characterized by three-dimensional periodic boundary conditions (volume of porous medium to be reconstructed) at a number density $N/V = (1-\phi)/(\pi\sigma^3/6)$, ensuring that the correct porosity will be achieved under the conditions of nonoverlap. The system of spheres is brought to a liquidlike disordered configuration by canonical (NVT) Monte Carlo simulation at a temperature of $T = \epsilon/k_B = 300$ K. The energy of the system is then minimized with respect to the coordinates of the sphere centers and an amorphous packing of soft spheres in detailed mechanical equilibrium is thereby created. In a second stage of the calculation, each sphere is converted to a rigid collection of eight smaller tangent spheres with their centers lying at the apices of an octahedron [generation 1, see Fig. 2 (top)]: the size σ of the spheres in this generation is chosen so that the volume of the "filled" three-dimensional object bordered by the sphere surfaces and by the faces of the octahedron formed by the sphere centers equals the volume of the original sphere of generation 0 and therefore of the octahedral crystals being simulated. Random orientations are initially assigned to the octets of spheres of generation 1 that replace the spheres of generation 0. The energy of the system is again minimized, imposing the condition of detailed mechanical equilibrium at the level of generation 1.

In the subsequent stages of the calculation (generation G), the representation of the octahedral particles is refined in relation to that of generation $G-1$, again preserving the particle volume, and the energy is again minimized.[21] By repeating this procedure for a sufficiently high G, an assemblage of octahedra is obtained, represented as collections of soft repulsive spheres resting upon each other in detailed mechanical equilibrium, and respecting the desired porosity. In fact,

for G varying from 9 up to 15 the faces of the objects are practically indistinguishable from the planar equilateral triangles, and thus allow replacement by actual octahedra bounded by planes of the desired size [see Fig. 2 (bottom)], for the simulation of the catalytic bed.

B. Kinetic Monte Carlo simulation

KMC simulation is used to track molecular and Knudsen diffusion of pointlike molecules in the model bed of octahedral crystals, obtained through the particle-based reconstruction procedure so as to match the characteristics of experimental samples. Long trajectories of individual sorbate molecules in the intercrystalline space are tracked by kinetic Monte Carlo simulations. The simulation observable is the mean square displacement as a function of time. Observation times are long, such that the displacement exceeds the size of individual crystals by at least an order of magnitude. The computations, carried out under the conditions of thermodynamic equilibrium, consider transport only in the intercrystalline spaces, assuming that molecules sorbed within the zeolite crystals are too slow to contribute to the long-range diffusion ($p_{\text{intra}}D_{\text{intra}} \ll p_{\text{inter}}D_{\text{inter}}$).

The KMC method is used in this work for the calculation of the self-diffusivity of ethane in the bed of NaX crystals, by computing the mean square displacement of a fixed number of molecules as they move in the intercrystalline space of the bed and hence the intercrystalline self-diffusivity D_{inter} by means of Eq. (3). NaX crystals are modeled as nonsorbing impermeable bodies in the present part of this study. The molecules, with mass m, at absolute temperature T, are assumed to travel with the mean thermal speed, $\bar{u} = (8k_BT/\pi m)^{1/2}$, given by the Maxwell velocity distribution.[22] A random change in the direction of motion occurs after any molecule-molecule collision. Such collisions are treated in a mean field sense, without explicitly considering colliding pairs; the distance l traveled between successive collisions is picked from an exponential distribution under the prevailing temperature T and pressure p, that is to say random trajectories are generated in the void space of the medium in such a way that in the bulk gas the lengths l between successive collisions follow the exponential distribution expected from the Poisson stochastic sequence of intermolecular collisions,[22]

$$\langle l \rangle f(l) = \exp(-l/\langle l \rangle), \tag{7}$$

where $f(l)dl$ is the conditional probability of having a collision-free trajectory length between l and $l+dl$, with the mean value of l being denoted by $\langle l \rangle$. In the bulk gas phase, $\langle l \rangle$ is the molecular mean free path

$$\lambda = \frac{k_BT}{p\sigma_{\text{gas}}^2 \pi \sqrt{2}}, \tag{8}$$

with σ_{gas} being the collision diameter of gas molecules.

Reflections upon collision with the isotropic crystal surface are assumed to be diffuse; that is to say, a new direction of motion is generated according to the cosine law[4] that ensures equal flux of the emitted molecules from the surface through any elementary area surrounding the collision point, irrespective of direction. The reflected trajectory vector is sampled from the probability density function $g(\vartheta, \psi)$, with ϑ and ψ being the polar and azimuthal angles, respectively, determining a solid angle $\sin\vartheta d\vartheta d\psi$ out of the surface. The fraction of particles leaving the surface with trajectories inside the range $(\vartheta, \vartheta+d\vartheta)$ and $(\psi, \psi+d\psi)$, is given by the following relation, normalized so that $\vartheta \in (0, \pi/2)$ and $\psi \in (0, 2\pi)$:

$$g(\vartheta, \psi)d\vartheta d\psi = -d\cos^2\vartheta d(\psi/2\pi). \tag{9}$$

In this way it is ensured that the probability for a molecule to leave the surface per unit time per unit area on the surface increases as the angle of reflection approaches the normal to the surface.

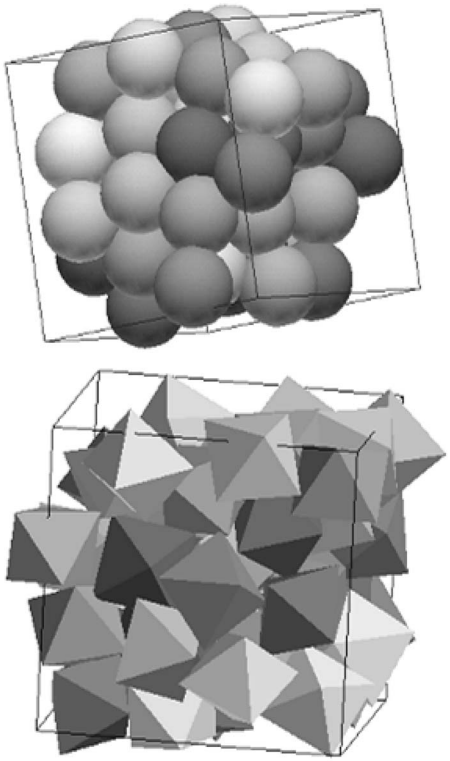

FIG. 3. Reconstructed bed of zeolite NaX; generation $G=0$ (top) generation $G=15$ (bottom).

IV. RESULTS AND DISCUSSION

Figure 3 (top) displayed the result of the reconstruction procedure for a bed of spherical crystals of NaX in mechanical equilibrium (generation 0), after the molecular mechanics-based minimization procedure, to reproduce the structural characteristics observed in the experimental part of this work.

Figure 3 (bottom) presented the results of the reconstruction for the bed of the NaX crystals used for the PFG NMR measurements (Fig. 1), as obtained from a sequence of successive energy minimizations starting from the coarse structure depicted at the top of the same figure and ending at generation 15.

The reconstruction procedure was repeated using the same size and shape (octahedral) of crystallites at a lower value of the porosity, $\phi=0.43$. The procedure in this case

TABLE I. Characteristics of the reconstructed NaX beds obtained through the molecular mechanics-based minimization procedure.

Crystal geometry	Simulation box length (μm)	Particle size (μm)	ϕ	Final G
Spherical	116.740	28.969 (diameter)	0.60	0
Octahedral	101.969	29.477 (edge)	0.43	11
Octahedral	116.740	29.996 (edge)	0.60	15

ended at generation 11, because of the slow convergence rate of the minimization algorithm as the void fraction of the system decreases. The characteristics of the reconstructed beds appear in Table I.

For each value of the porosity reported in Table I, 20 different configurations were generated by repeating the minimization from a different, independently generated, starting point configuration. Separate kinetic Monte Carlo simulation experiments were performed in every reconstructed structure.

Figures 4 and 5 display the intercrystalline self-diffusivity of ethane, calculated as an average over a large number of single-molecule trajectories generated in 20 different realizations of the porous structure as described above, as a function of mean free path λ and Knudsen number Kn $=\lambda/d_s$ at 295 K in a series of reconstructed beds of $\phi=0.60$ and 0.43, respectively. In the original definition of Kn, d_s is the diameter of a tube of infinite length wherein molecular motion takes place. In studies of transport phenomena inside porous media d_s is estimated as the mean length, $\langle d_s\rangle$, of random secants through the void space of the porous material of total volume V which comprises a solid phase of surface area S as follows:

$$\langle d_s\rangle = \frac{4\phi V}{S}. \tag{10}$$

Let us define the mean surface-to-surface path length, $\langle l\rangle$, as the mean free path between collisions with the walls in

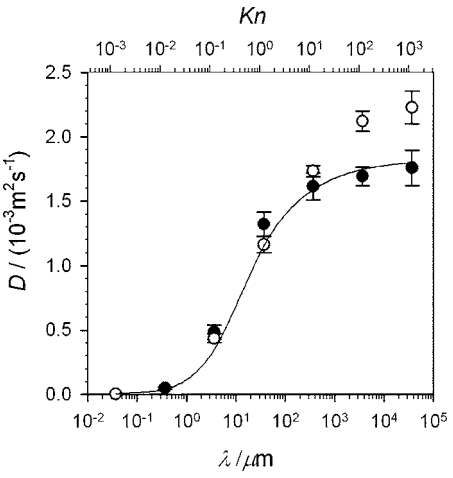

FIG. 4. Intercrystalline self-diffusivity of ethane computed via kinetic Monte Carlo simulation in a reconstructed bed of spherical ($G=0$) NaX pseudocrystals (open symbols); in a reconstructed ($G=15$) bed of octahedral NaX crystals (filled symbols); and calculated via Eq. (13) for the bed of octahedral crystals (line), as a function of mean free path λ and Knudsen number Kn, at porosity $\phi=0.60$.

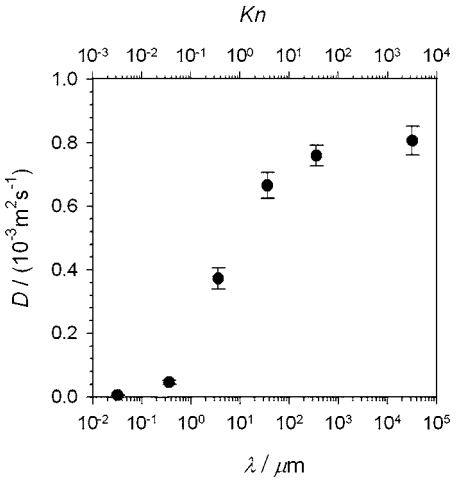

FIG. 5. Same as Fig. 4 for a bed of octahedral NaX crystals ($G=11$) of $\phi=0.43$.

the Knudsen diffusion regime for a particle traveling inside the void space without penetrating the solid phase of a porous medium,

$$\langle l\rangle_{\mathrm{Kn}\gg 1} = \frac{1}{\phi V}\int \bar{d}_s(\mathbf{r})d^3r, \tag{11}$$

where the quantity $\bar{d}_s(\mathbf{r})$ represents an average over all possible directions emanating from a point $\mathbf{r}$, with d^3r being an element of volume about this point. The integral is taken over the entire void space of the medium so that Eq. (11) expresses an average of the mean surface-to-surface paths over all points belonging to ϕV and over all directions.

Kingman's work[23] on the acoustical design of auditoria, assuming perfectly reflecting walls and invoking the Birkhoff ergodic theorem, resulted mathematically in the following equation for the mean free path of sound:

$$\langle l\rangle = \frac{4\phi V}{S} + \frac{S}{4\phi V}\mathrm{var}[\bar{d}_s(\mathbf{r})]. \tag{12}$$

This equation elicits a position dependent $\bar{d}_s(\mathbf{r})$ because of the nonergodicity of the reflected trajectories as a consequence of the shape of the interior region only, without taking into account the nature of collisions with the surfaces. Obviously, if $\bar{d}_s(\mathbf{r})$ is independent of the point of emission ($\mathrm{var}[\bar{d}_s(\mathbf{r})]=0$), then $\langle l\rangle=\langle d_s\rangle$, thus, Eq. (12) takes the simple form of Eq. (10).

Assuming negligible overlap between the solid objects in the reconstructed beds, a fact ensured by the nature of the steeply repulsive potential employed during the minimization procedure, $\langle d_s\rangle$ was estimated using the forms of Eq. (10) listed in the footnotes of Table II. The surface-to-surface path length, $\langle l\rangle$, formally defined in Eq. (11), was estimated directly as the mean free path $\langle l\rangle_{\mathrm{Kn}\gg 1}$ from the KMC simulations in the Knudsen regime. Clearly, the agreement between the mathematical formalism of Eqs. (10) and (12) and the corresponding physical analog of Eq. (11) compared in Table II shows that the variance of $\bar{d}_s(\mathbf{r})$, which now incorporates the reflection type adopted in our simulations

TABLE II. Mean intercept lengths in the reconstructed NaX zeolite beds: calculated via Eq. (10), computed via simulation of intercrystalline diffusion in the Knudsen regime, and experimental vs simulated tortuosity ratios using Eqs. (15) and (21) for the same reconstructed media.

ϕ	$\langle d_s \rangle$ (μm)	$\langle l \rangle_{\mathrm{Kn}\gg 1}$ (μm)	$\eta_{\mathrm{Kn}}/\eta_b$ PFG NMR	$\eta_{\mathrm{Kn}}/\eta_b$ Simulation[a]	β	$\langle l^2 \rangle_{\mathrm{Kn}\gg 1}/2\langle l \rangle^2_{\mathrm{Kn}\gg 1}$ Simulation[a]	$\eta_{\mathrm{Kn}}/\eta_{b\ \mathrm{corrected}}$
0.60 (sph)	26.511[b]	26.350	⋯	1.55	0.309	0.935	0.97
0.60 (oct)	24.492[c]	24.320	4.7–10[d]	2.04	0.298	0.849	1.12
0.43 (oct)	12.104[c]	12.134	⋯	2.14	0.270	0.866	1.28

[a]Reported ratios are subject to error bars varying from ±8% to ±13%.
[b]Value calculated from Eq. (10) read as $2d_i\phi/3(1-\phi)$; d_i sphere diameter.
[c]Value calculated from Eq. (10) read as $2a_i\phi\sqrt{6}/9(1-\phi)$; a_i octahedron edge.
[d]Range resulting from the uncertainty of the experimental porosity of 0.60±0.15, (Ref. 25), as it is propagated in the calculation of $\langle d_s \rangle$.

through Eq. (9), practically vanishes, clarifying this way the conditions under which the relation $\langle l \rangle_{\mathrm{Kn}\gg 1}=\langle d_s \rangle$ is obeyed in disordered porous media.[24]

On the left-hand side of Figs. 4 and 5 is seen the high-pressure regime ($\langle l \rangle=\lambda, \mathrm{Kn}\ll 1$) where the overall diffusion process is controlled by frequent intermolecular collisions, leading to small mean free paths. The calculated interparticle diffusivity in this regime can be identified with an effective bulk diffusion coefficient, D_b. On the right-hand side of the same graphs we see the low-pressure regime, where molecular collisions with the surfaces of crystals in the bed dominate the overall diffusion process and mean free paths are long ($\langle l \rangle \ll \lambda, \mathrm{Kn}\gg 1$); hence, the calculated long-range diffusivity can be identified in a similar way with an effective Knudsen diffusivity, D_{Kn}. The effective intercrystalline diffusivity, D_{inter}, over the whole range of pressures (or Knudsen numbers), may be estimated through the Bosanquet approximation[4] as a harmonic mean of the diffusivities D_b and D_{Kn}, associated with the two aforementioned limiting situations, as follows:

$$D_{\mathrm{inter}}^{-1} = D_{\mathrm{Kn}}^{-1} + D_b^{-1}. \tag{13}$$

Estimates of D_{inter} based on Eq. (13) in the bed of octahedral crystals at $\phi=0.60$ are shown in Fig. 4 (line); the Bosanquet approximation leads to a small underestimation of the effective diffusivity in the transition region.

As mentioned in the previous section, only an overall (long-range) diffusivity, D_{LR}, is measured via PFG NMR, which in general includes contributions from intracrystalline diffusion, surface diffusion, sorption, and desorption phenomena in addition to Knudsen and molecular diffusion in the macropores. [Compare Eq. (4) and the discussion that follows it.] On the other hand, the simulation performed at the current stage involves a bed of impermeable zeolite crystals. Since the PFG NMR cannot directly measure bulk or Knudsen diffusivity, in the experiment both magnitudes were extracted from D_{LR} through the proper fraction p_{inter} in each case.[19,25] The fraction p_{inter} was calculated on the assumption that Henry's law applies in the system under study. The latter assumption has been experimentally verified in previous work,[19,25] ensuring that $c_{\mathrm{intra}} \gg c_{\mathrm{inter}}$, and $c_{\mathrm{intra}}=K_H p$ for the entire pressure range used in this work; K_H is the Henry constant. For the experimental temperature range of 193–368 K used here, the calculated values of the ethane pressure varied from 10^{-1} to 7.0×10^2 mbars, with p_{inter} values being in the range of 2.0×10^{-5} to 5.0×10^{-2}, respectively.

Although the absolute values of the estimates for bulk, $D_b=D_{\mathrm{inter}}(\mathrm{Kn}\ll 1)$, and Knudsen, $D_{\mathrm{Kn}}=D_{\mathrm{inter}}(\mathrm{Kn}\gg 1)$, diffusivities extracted from the PFG NMR depend strongly on the sorption isotherm, a comparison with the corresponding quantities predicted from simulation can be made on the basis of the relative deviations from the reference diffusivities D_{0b} and $D_{0\mathrm{Kn}}$ expected to prevail in the purely molecular diffusion-dominated and purely Knudsen diffusion-dominated regimes, respectively. Following the definitions

$$D_{0b} = \frac{1}{3}\bar{u}\lambda \tag{14}$$

and

$$D_{0\mathrm{Kn}} = \frac{1}{3}\bar{u}\langle l \rangle_{\mathrm{Kn}\gg 1}, \tag{15}$$

the tortuosities η_b and η_{Kn} in the two regimes can then be defined[26] as

$$\eta_b = \frac{D_{0b}}{D_b}\phi \tag{16}$$

and

$$\eta_{\mathrm{Kn}} = \frac{D_{0\mathrm{Kn}}}{D_{\mathrm{Kn}}}\phi. \tag{17}$$

In elaborating PFG NMR diffusivity data to extract tortuosities, the above expressions have been treated[19,25] with $\phi=1$, whereas in simulation the actual macropore void fraction has been used as ϕ. Nevertheless, when comparison between experiment and simulation is performed on the basis of ratios $\eta_{\mathrm{Kn}}/\eta_b$, the dependence on porosity is factored out. In Table II it is shown that both predicted and measured ratios indicate a significantly higher tortuosity factor in the Knudsen diffusion regime than in the bulk regime. The departure of the ratio from unity tends to be stronger in the simulated bed of porosity 0.43, suggesting that tortuosities in the Knudsen regime increase in relation to those in the molecular regime as the void fraction decreases; this trend is in agreement with previous simulation studies on even more compacted structures of randomly packed hard spheres[9] with $\phi=0.38$, or overlapping spheres[27] with ϕ varying from 0.06 to 0.042, as well as in pixelized porous media.[28]

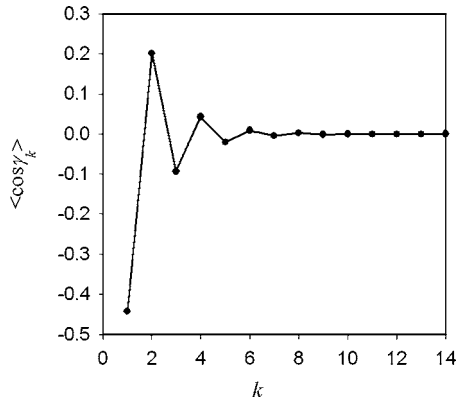

FIG. 6. Average cosine values of vector angles in Eq. (19) as a function of the number of intervening collisions k for the bed of octahedral crystals at $\phi=0.60$.

It must be noted here that the bed of lower void fraction $\phi=0.43$ was modeled in order to capture the behavior of the experimentally used bed of $\phi=0.60\pm0.15$ over its whole range of variation; the reconstruction of a model bed of $\phi=0.75$ leads to unrealistically loose structures of NaX crystals, far from being in contact.

Through a further elaboration of Eq. (3), by regarding the vector $\mathbf{r}$ traveled by a random walker during time t as the vector sum of n rectilinear segments, $\mathbf{l}_i$, traversed between collisions, one arrives to the following expression:

$$\mathbf{r}^2 = \sum_{i=1}^{n} \mathbf{l}_i^2 + 2\sum_{i=1}^{n-1} \sum_{j=i+1}^{n} \mathbf{l}_i \cdot \mathbf{l}_j. \tag{18}$$

Since vectors are no more correlated directionally after a small number of collisions (see Fig. 6), following the work of Derjaguin[29] on the Knudsen flow of rarefied gases through a porous medium, the average of Eq. (18) for $n \gg 1$ gives

$$\langle \mathbf{r}^2 \rangle \approx n\langle l^2 \rangle + 2\left\langle \sum_{i=1}^{n} l_i \sum_{j=1}^{\infty} l_{i+j} \cos \gamma_{i,i+j} \right\rangle,$$

with $\gamma_{i,i+j}$ being the angle between vectors $\mathbf{l}_i$ and $\mathbf{l}_{i+j}$. Assuming, in addition, mutual independence of the lengths l_i, l_{i+j} and the angle $\cos \gamma_{i,i+j}$ the above average transforms to

$$\langle \mathbf{r}^2 \rangle \approx n\langle l^2 \rangle + 2n\langle l \rangle^2 \sum_{k=1}^{\infty} \langle \cos \gamma_k \rangle, \tag{19}$$

where the sum on the right-hand side runs over all average cosines between segments $\mathbf{l}_i$ separated by k collisions. This sum can be computed readily from a simulation trajectory in a manner entirely analogous to the computation of mean square displacement using multiple time origins.

Combining Eqs. (3) and (19) and using the fact that the total trajectory length $n\langle l \rangle$ divided by the total elapsed time t equals the mean velocity $\bar{u}$ lead us to a comprehensive relation for the self-diffusivity over the entire diffusion regime, i.e.,

$$D = \frac{1}{3}\bar{u}\langle l \rangle \left[\frac{\langle l^2 \rangle}{2\langle l \rangle^2} - \beta \right] \tag{20}$$

with

$$\beta = -\sum_{k=1}^{\infty} \langle \cos \gamma_k \rangle.$$

Intermolecular collisions in the gas phase follow an exponential distribution in l, as described by Eq. (7). For such a distribution, the ratio of moments is $\langle l^2 \rangle / 2\langle l \rangle^2 = 1$. In addition, no directional correlation between successive trajectory segments is expected, hence $\beta=0$; therefore, in the molecular diffusion-dominated regime Eq. (20) reduces to Eq. (14).

Specializing now to the Knudsen regime, Eq. (20) becomes

$$D_{0\mathrm{Kn}} = \frac{1}{3}\bar{u}\langle l \rangle_{\mathrm{Kn}\gg1} \left[\frac{\langle l^2 \rangle_{\mathrm{Kn}\gg1}}{2\langle l \rangle_{\mathrm{Kn}\gg1}^2} - \beta \right]. \tag{21}$$

As seen in Table II on the basis of computed trajectories, the ratio $\langle l^2 \rangle_{\mathrm{Kn}\gg1} / 2\langle l \rangle_{\mathrm{Kn}\gg1}^2$ in the Knudsen diffusion regime can vary from 0.8 to 1, depending on the interfacial geometry of the objects constituting the bed, and exhibiting no significant dependence on the porosity. In Fig. 6 the successive terms constituting β are examined for the bed of tetrahedral particles at $\phi=0.60$. Significant directional correlation is observed; $\langle \cos \gamma_k \rangle$ is seen to exhibit damped oscillations around 0, which die out after about eight collisions with the surface of the octahedra with the diffuse reflection rule applied [see Eq. (9)]. The β values do not appear to exhibit any systematic dependence on the porosity.

Using the $D_{0\mathrm{Kn}}$ given by the corrected Eq. (21) as a reference diffusivity in place of Eq. (15), the ratio of Knudsen over bulk regime tortuosity reads

$$\left. \frac{\eta_{\mathrm{Kn}}}{\eta_b} \right|_{\mathrm{corrected}} = \frac{\eta_{\mathrm{Kn}}}{\eta_b} \left[\frac{\langle l^2 \rangle_{\mathrm{Kn}\gg1}}{2\langle l \rangle_{\mathrm{Kn}\gg1}^2} - \beta \right]. \tag{22}$$

In Table II it is seen that the corrected values of this ratio are in all cases indistinguishable from unity within the statistical error of the simulation.

Zalc *et al.*[27] observed a decrease of β for randomly packed spheres as the porosity was changed from 0.42 to 0.07; the correlation between segments of trajectories reflected from the surfaces became more pronounced as the void fraction available for interparticle diffusion in the medium decreased. In their study, the ratio $\langle l^2 \rangle_{\mathrm{Kn}\gg1} / 2\langle l \rangle_{\mathrm{Kn}\gg1}^2$ remained close to unity, so that the correction to the reference Knudsen self-diffusivities through Eq. (21) was made merely through the β values.

In order to study the effect of interfacial geometry on the distribution of the vectors $\mathbf{l}_i$ as well as on their degree of orientational correlation under the same reflection rule from the surface, diffusion simulation studies were carried out in a bed of spherical particles of the same porosity $\phi=0.60$ (Fig. 4, first row of Tables I and II). As seen in Table II, the factor $\langle l^2 \rangle_{\mathrm{Kn}\gg1} / 2\langle l \rangle_{\mathrm{Kn}\gg1}^2$ was found practically equal to unity. On the contrary, β was found to deviate considerably from 0. The corrected ratio of tortuosities in the bed of spherical pseudocrystals was again very close to 1. These findings are in conformity to the results of Zalc *et al.*[27] Comparison between the simulation results reported in Table II suggests that

the distribution of molecular paths deviates from being exponential [Eq. (7)] as particles constituting the bed depart from the spherical shape.

V. CONCLUSION

A comparison of kinetic Monte Carlo simulations and PFG NMR measurements of the long-range diffusivity of ethane in a bed of NaX zeolite crystals was carried out in the molecular, transient, and Knudsen diffusion regimes. For the digital representation of the experimental bed of zeolite crystals, a novel reconstruction technique was used at two porosity values of 0.60 and 0.43 to capture the experimental range of uncertainty in the porosity. Only interparticle diffusion in the macropores was studied in the simulations, as this, as opposed to intracrystalline diffusion, dominated the PFG NMR measurements. In the simulations, diffuse reflection from the zeolite crystal surfaces was postulated, with the direction of reflected molecular trajectories following a cosine law.

The results of PFG NMR revealed a strong dependence of the apparent tortuosity factors on the regime of diffusion, tortuosities in the Knudsen regime being by a factor of 4.7–10 higher than tortuosities in the molecular diffusion-dominated regime.

The predicted tortuosity ratios in the reconstructed beds were in qualitative agreement with experiment. Using the conventional, experimentally accessible definition of tortuosities, they yielded tortuosity values that were higher in the Knudsen regime than in the molecular diffusion-dominated regime by a factor of about 2. With the usual definition of tortuosity factors, contrary to common belief, they are not unique functions of the structure of the medium, but also depend on the regime of diffusion.

Examining, furthermore, the statistics of molecular trajectories in the Knudsen diffusion regime in a manner suggested by the work of Derjaguin,[29] in terms of the two first moments of the distribution of segment lengths between collisions with the solid and of the directional correlation between these segments, we were able to define corrected tortuosity factors for the Knudsen regime. Correspondingly, corrected tortuosity ratios between the Knudsen and molecular diffusion-dominated regimes could be formulated [Eq. (22)]. These corrected diffusivity ratios were indistinguishable from unity. Thus, if tortuosity in the Knudsen regime is defined in terms of a reference diffusivity that takes into account the departure of actual molecular trajectories from their usually postulated statistical characteristics, the same value is obtained as in the molecular diffusion-dominated regime and the puzzle of regime-dependent tortuosity factors is resolved. Such a corrected definition of tortuosity cannot be easily implemented in experimental work, as it requires knowledge of the detailed geometric characteristics of molecular trajectories.

[1] J. Crank, *The Mathematics of Diffusion*, 2nd ed. (Clarendon, Oxford, 1975).
[2] R. M. Barrer, Appl. Mater. Res. **2**, 129 (1963).
[3] R. M. Barrer, in *Surface and Volume Flow in Porous Media*, The Solid-Gas Interface, Vol. 2, edited by E. A. Flood (Dekker, New York, 1967).
[4] R. E. Cunningham and R. J. J. Williams, *Diffusion in Gases and Porous Media* (Plenum, New York, 1980).
[5] D. ben-Avraham and S. Havlin, *Diffusion and Reactions in Fractals and Disordered Systems* (Cambridge University Press, Cambridge, 2000).
[6] E. A. Mason and A. P. Malinauskas, *Gas Transport in Porous Media: The Dusty-Gas Model* (Elsevier, New York, 1983).
[7] D. Nicholson and J. H. Petropoulos, J. Phys. D **10**, 2423 (1977).
[8] M. M. Tomadakis and S. V. Sotirchos, AIChE J. **37**, 74 (1991).
[9] P. Levitz, J. Phys. Chem. **97**, 3813 (1993).
[10] G. K. Papadopoulos and J. H. Petropoulos, J. Chem. Soc., Faraday Trans. **92**, 3217 (1996).
[11] J. W. Evans, M. H. Abbasi, and A. Sarin, J. Chem. Phys. **72**, 2967 (1980).
[12] V. Burganos and S. V. Sotirchos, Chem. Eng. Sci. **43**, 1685 (1988).
[13] V. Burganos and S. V. Sotirchos, Chem. Eng. Sci. **44**, 2629 (1989).
[14] R. R. Melkote and K. F. Jensen, AIChE J. **35**, 1942 (1989).
[15] M. M. Tomadakis and S. V. Sotirchos, AIChE J. **39**, 397 (1993).
[16] K. Makrodimitris, G. K. Papadopoulos, C. Philippopoulos, and D. N. Theodorou, J. Chem. Phys. **117**, 5876 (2002).
[17] J. Kärger and D. M. Ruthven, *Diffusion in Zeolites and Other Microporous Solids* (Wiley-Interscience, New York, 1992).
[18] G. K. Papadopoulos, H. Jobic, and D. N. Theodorou, J. Phys. Chem. B **108**, 12748 (2004).
[19] O. Geier, S. Vasenkov, and J. Kärger, J. Chem. Phys. **117**, 1935 (2002).
[20] D. N. Theodorou and U. W. Suter, Macromolecules **18**, 1467 (1985).
[21] G. K. Papadopoulos and D. N. Theodorou (unpublished).
[22] E. H. Kennard, *Kinetic Theory of Gases* (McGraw-Hill, New York, 1938).
[23] J. F. C. Kingman, J. Appl. Probab. **2**, 162 (1965).
[24] S. Torquato, *Random Heterogeneous Materials, Microstructure and Macroscopic Properties* (Springer-Verlag, New York, 2002).
[25] S. Vasenkov, O. Geier, and J. Kärger, Eur. Phys. J. E **12**, S35 (2003).
[26] C. N. Satterfield, *Mass Transport in Heterogeneous Catalysis* (MIT, Cambridge, 1970).
[27] J. M. Zalc, S. C. Reyes, and E. Iglesia, Chem. Eng. Sci. **59**, 2947 (2004).
[28] V. N. Burganos, J. Chem. Phys. **109**, 6772 (1998).
[29] B. Derjaguin, C. R. (Dokl.) Acad. Sci. URSS **7**, 623 (1946).